Asymmetric Coupling Effects in the Synchronization of Spatially Extended Chaotic Systems

J. Bragard,[1] S. Boccaletti,[2] and H. Mancini[1]

[1]*Department of Physics and Applied Mathematics, University of Navarre, Pamplona, Spain*
[2]*Istituto Nazionale di Ottica Applicata, Largo E. Fermi, 6, 50125 Florence, Italy*

We analyze the effects of asymmetric couplings in setting different synchronization states for a pair of unidimensional fields obeying complex Ginzburg-Landau equations. Novel features such as asymmetry enhanced complete synchronization, limits for the appearance of phase synchronized states, and selection of the final synchronized dynamics are reported and characterized.

PACS numbers: 05.45.Jn, 05.45.Xt

The synchronization of coupled chaotic systems has attracted increasing attention over the past few years. Different synchronization features have been described for coupled confined systems [1] and later were explored in natural phenomena [2] and laboratory experiments [3].

More recently, the interest moved to the study of synchronization phenomena in space-extended systems, such as large populations of coupled chaotic units and neural networks [4], globally or locally coupled map lattices [5], and continuous systems ruled by partial differential equations [6–8].

So far, studies on synchronization of chaos have mainly focused on external forcings and bidirectional symmetric or unidirectional master-slave coupling schemes. However, in nature we cannot expect to have purely unidirectional or perfectly symmetrical coupling configurations. Therefore, our intention in this Letter is to address the effects of asymmetries in the coupling of space-extended continuous fields.

We refer to a pair of unidimensional fields obeying complex Ginzburg-Landau equations. This equation, indeed, has been extensively investigated in the context of space-time chaos, since it describes the universal dynamical features of an extended system close to a Hopf bifurcation [9], and therefore it can be considered as a good model equation for many different physical situations, such as laser physics [10], fluid dynamics [11], chemical turbulence [12], bluff body wakes [13], etc.

The system under study is

$$\dot{A}_{1,2} = A_{1,2} + (1 + i\alpha)\partial_x^2 A_{1,2} - (1 + i\beta_{1,2})|A_{1,2}|^2 A_{1,2}$$
$$+ \frac{c}{2}(1 \mp \theta)(A_{2,1} - A_{1,2}). \qquad (1)$$

Here $A_{1,2}(x, t) = \rho_{1,2}(x, t)e^{i\phi_{1,2}(x, t)}$ are two complex fields [of amplitudes $\rho_{1,2}(x, t)$ and phases $\phi_{1,2}(x, t)$], dots denote temporal derivatives, ∂_x^2 stays for the second derivative with respect to the space variable $0 \leq x \leq L$, L is the system extension, α and $\beta_{1,2}$ are suitable real parameters, c represents the coupling strength, and θ is a parameter accounting for asymmetries in the coupling. Precisely, the case $\theta = 0$ recovers the bidirectional symmetric coupling configuration, whereas the case $\theta = 1$

($\theta = -1$) recovers the unidirectional master-slave scheme, with the field A_1 (A_2) driving the response of A_2 (A_1).

In the uncoupled case ($c \equiv 0$), different regimes are set in Eqs. (1) for different choices of the parameters α, $\beta_{1,2}$ [14], depending on the stability properties of the plane wave solutions (PWS) $A_q = \sqrt{1 - q^2}e^{i(qx+\omega t)}$ [$-1 \leq q \leq 1$, q being the wave number in Fourier space, $\omega = -\beta - (\alpha - \beta)q^2$]. Namely, for $\alpha\beta > -1$ a critical wave number $q_c = \sqrt{(1 + \alpha\beta)/[2(1 + \beta^2) + 1 + \alpha\beta]}$ exists such that all PWS in the range $-q_c \leq q \leq q_c$ are linearly stable. Outside this range, PWS become unstable through the Eckhaus instability [15]. When crossing from below the Benjamin-Feir line $\alpha\beta = -1$ in the parameter space, q_c vanishes and all PWS become unstable. Above this line, Ref. [14] describes different turbulent regimes. For the scope of this work, we mainly concentrate on phase turbulence (PT) and amplitude turbulence (AT) or defect turbulence.

PT is a regime where the chaotic behavior of the field is mainly dominated by the dynamics of $\phi(x, t)$, while the amplitude changes smoothly, and it is always bounded away from zero. At variance, in AT the fluctuations of $\rho(x, t)$ become dominant over the phase dynamics, leading to large amplitude oscillations which can occasionally cause the occurrence of space-time defects in points where ρ is locally vanishing.

By selecting in (1) a sufficiently large parameter mismatch in the equations for $A_{1,2}$, one can set the uncoupled evolutions of A_1 and A_2 to be in PT and AT, respectively. In these conditions, the case $\theta = 0$ was extensively studied in Ref. [7], where completely synchronized PT states were seen to emerge as a consequence of increasing the coupling strength, while the case $\theta = 1$ was considered in Ref. [8], where both complete and phase synchronization features were discussed and characterized.

In the following we consider all values of $\theta \in [-1, +1]$ and highlight the effects of asymmetries in the synchronization properties of system (1). Simulations were performed with a Crank-Nicholson, Adams-Bashforth scheme (which is second order in space and time [16]), with a time step $\delta t = 10^{-2}$ and a grid size

$\delta x = 0.25$, for $L = 100$ (corresponding to 400 grid points) and spatial periodic boundary conditions $[A_{1,2}(0, t) = A_{1,2}(L, t)]$.

Let us start by discussing how to characterize the synchronization properties of the coupled fields by means of suitable indicators [8].

In order to reveal 1:1 phase synchronization (PS), instead of using the phases $\phi_{1,2}(x, t) \in [0, 2\pi]$, we make reference to the unfolding of the phases to the real axis $[\phi_{1,2}(x, t) \in R]$. This way, 1:1 PS holds if the following condition is satisfied:

$$\Delta\phi = \max_{x \in L, T \leq t \in R} |\phi_1(x, t) - \phi_2(x, t)| < K, \quad (2)$$

where T denotes a transient time and K is a suitable real number. Condition (2) implies that the maximum relative phase difference remains bounded for all times. In (2), we introduce a transient time T, which allows us to get rid of all transient effects (in the present case $T = 4000$). Even though formally Eq. (2) can be considered as a proper indicator for PS only within phase turbulent regimes, we follow the same strategy as [8] of using it also for measuring intermediate PS states displaying AT.

An alternative measure of frequency locking can be obtained by monitoring the mean frequency mismatch. The mean frequency of each field is given by $\Omega_{1,2} = \lim_{t \to \infty} \frac{\langle \phi_{1,2}(x,t) \rangle_x}{t}$, where $\langle \rangle_x$ denotes spatial average. 1:1 frequency synchronization (FS) occurs when

$$\Delta\Omega = \Omega_1 - \Omega_2 = 0. \quad (3)$$

It is important to notice that condition (3) represents a weaker form of phase locking. Indeed, while PS implies FS, the opposite does not hold in general, because the evolution of $\Delta\phi$ might be affected by 2π phase slips over secular time scales, which are averaged out in the frequency definition.

As for complete synchronization (CS) states, they can be detected by monitoring the Pearson's coefficient γ, which measures the degree of cross correlation between the moduli $\rho_{1,2}(x, t)$ (once again after the transient time T),

$$\gamma = \frac{\langle (\rho_1 - \langle \rho_1 \rangle)(\rho_2 - \langle \rho_2 \rangle) \rangle}{\sqrt{\langle (\rho_1 - \langle \rho_1 \rangle)^2 \rangle} \sqrt{\langle (\rho_2 - \langle \rho_2 \rangle)^2 \rangle}}, \quad (4)$$

where $\langle \rangle$ denotes a full space-time average.

Precisely, when $\gamma \simeq 0$ the two fields are linearly uncorrelated; $\gamma = 1$ marks complete correlation and $\gamma = -1$ indicates that the fields are negatively correlated.

Another indicator for the disorder in the system is the number of phase defects N. Theoretically, a defect is a point (x, t) for which $\rho(x, t) \to 0$; i.e., defects are intersections of the zero-level curves in the (x, t) plane of the real and imaginary parts of $A_{1,2}(x, t)$. In practice, because of the finite size of the mesh, we count as defects at time t those points x_i where the $\rho(x_i, t)$ is smaller than 2.5×10^{-2} and that are furthermore local minima for the function $\rho(x, t)$. It is well known that N is an extensive

quantity of both time and space, and therefore it is sometimes convenient to refer to the defect density n_D, which is calculated as the defect number N per unit time and unit space.

Let us move now to describe the effects of asymmetry in the coupling in system (1). For that purpose, we select $\alpha = 2$, $\beta_1 = -0.7$, and $\beta_2 = -1.05$, which corresponds to set the uncoupled evolution of A_1 (A_2) in PT (AT). In all cases, the different synchronization indicators are evaluated over a time $t = T + 6000$.

Figure 1 reports the Pearson's coefficient values in the parameter space (c, θ) (a) as well as two cuts of the surface at $c = 0.25$ and $c = 0.6$ (b). The results indicate that the threshold for the appearance of a CS state depends crucially on the asymmetry θ in the coupling. In particular, Fig. 1 shows that asymmetry can enhance the occurrence of a synchronized motion.

Let us now move to discuss how asymmetry influences the selection of the final synchronized state. Looking at Fig. 2, one realizes that the CS state ($\gamma \simeq 1$) occurs in PT (no defects in both fields), for nearly all values of θ. This confirms the results already shown in Ref. [7] for $\theta = 0$ and indicates that the preferred state for complete synchronization is in the PT regime, except for θ very close to -1, where the AT system is driving the "slaved" PT
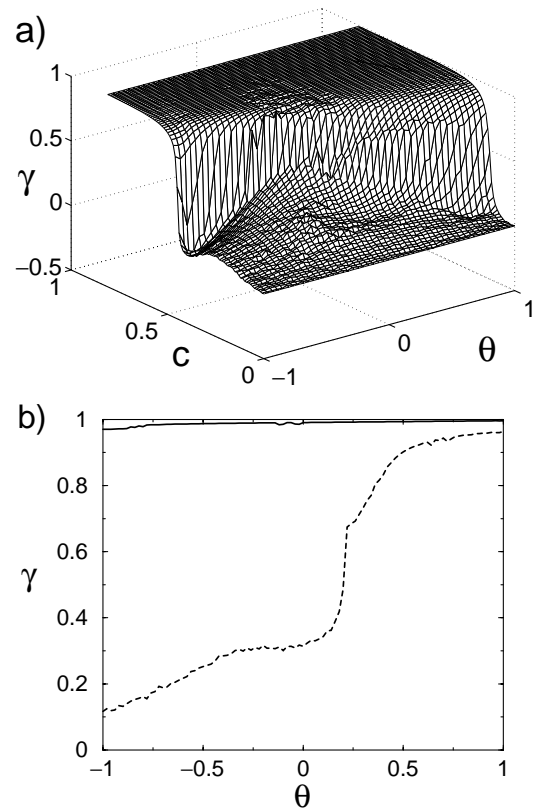

FIG. 1. (a) Pearson's coefficient γ (see text for definition) vs the parameter space (c, θ). Other parameters are $\alpha = 2$, $\beta_1 = -0.7$, and $\beta_2 = -1.05$. (b) Pearson's coefficient vs coupling asymmetry θ, for $c = 0.25$ (dashed line) and $c = 0.6$ (solid line).
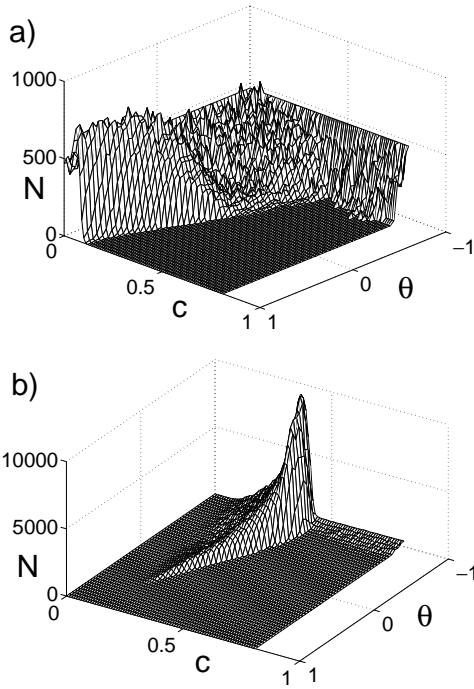
a)

b)

FIG. 2. Total number of defects N generated in the system A_2 (a) and A_1 (b) vs the parameter space (c, θ). Other parameters are as in the caption of Fig. 1. The density of space-time defects n_D can be obtained here by normalizing N to 6000×100 (time interval × space interval).

system. Even more interestingly, the final CS state is reached after an intermediate ($\gamma < 1$) AT state, where both systems display phase defects, and the number of defects in the field A_1 (that was originally set in PT) shows a kind of divergence for coupling strengths close but slightly below the threshold for CS [Fig. 2(b)]. Simulations performed at $c = 0.38$ and $\theta = -1$ with a system of larger extent $L = 1000$ show that the PT system [Fig. 3(a)] produces approximately 19 times more defects than the AT system [Fig. 3(b)] within the intermediate state.

Finally, we discuss how asymmetric couplings influence the settings of PS and FS states. Figure 4 reports the indicators for PS (a) and FS (b), as well as a plot of the maximum phase difference vs time (c) for the parameters $c = 0.6$ and $\theta = -0.9$. As already noticed for CS, the thresholds for the setting of PS and FS states depend on the asymmetry, and both synchronization features are enhanced for $\theta \Rightarrow 1$ [see Figs. 4(a) and 4(b)]. In the opposite limit ($\theta \Rightarrow -1$), by comparing Fig. 4(a) with Fig. 1, one realizes that PS is set for coupling strengths for which a CS state has already emerged in the system; thus the range for the existence of a PS regime is here shrunk. Eventually, for $\theta \simeq -1$, PS fails, due to the presence of defects in the final synchronized state.

At variance, FS states persist also for $\theta \simeq -1$ [see Fig. 4(b)]. This indicates how the two conditions for FS and PS point to different synchronization features, since they emerge from different measures of phase and fre-
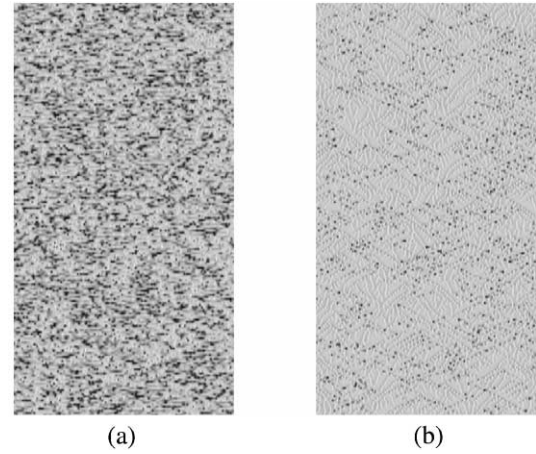
FIG. 3. Space-time plot of $\rho_1(x, t)$ (a) and $\rho_2(x, t)$ (b) for $c = 0.38$ and $\theta = -1$. Time is increasing upwards. Other parameters are as in the caption of Fig. 1.

quency synchronization. More insight on the limits for PS states can be extracted from Fig. 4(c). The upper left plot of Fig. 4(c) shows a maximum phase difference that increases linearly with time, as expected for parameters ($c = 0.2$, $\theta = -0.9$) for which FS fails. The lower left plot of Fig. 4(c) shows the maximum phase difference vs time for $c = 0.6$ and $\theta = -0.9$ (parameters for which FS is observed while PS fails). There, one can see that the system shows rather long epochs of phase locked states, interrupted by sudden 2π phase slips, that occur over secular time scales. The right plots report the corresponding spatial distributions of $\Delta\tilde{\phi}(x) = \mathrm{mod}_{2\pi}[\phi_1(x, t) - \phi_2(x, t)]$ mediated over many time realizations. While for $c = 0.2$ the distribution comes out to be quite homogeneous in $[0, 2\pi]$, at $c = 0.6$ a clear peak in $P(\Delta\tilde{\phi})$ indicates a preferred value in the phase difference holding over the 2π-stairlike behavior.

Another effect of asymmetry is the transition from normal to anomalous FS states, as can be seen in Fig. 4(b). "Anomalous" phase synchronization [17] indicates a situation in which increasing the coupling initially leads to a degradation of frequency locking. Here, for almost all θ(except for $\theta \approx 1$), an increase in c yields initially a higher frequency difference. After reaching a maximum, $\Delta\Omega$ eventually vanishes as c approaches the asymmetry dependent threshold for FS. This anomaly is intimately related to the preference of the system for a PT synchronized state. When θ approaches 1, the final synchronized state is reached by means of a smooth transition in $\Delta\Omega$, because the coupling scheme approaches the unidirectional configuration with the PT subsystem forcing the AT one. At variance, for the other values of θ, the final state is reached after an intermediate partially synchronized regime (see Figs. 2 and 3 and the above discussion), which is producing the anomaly in the FS transition.

In conclusion, we have addressed and studied several synchronization regimes in continuous space-extended
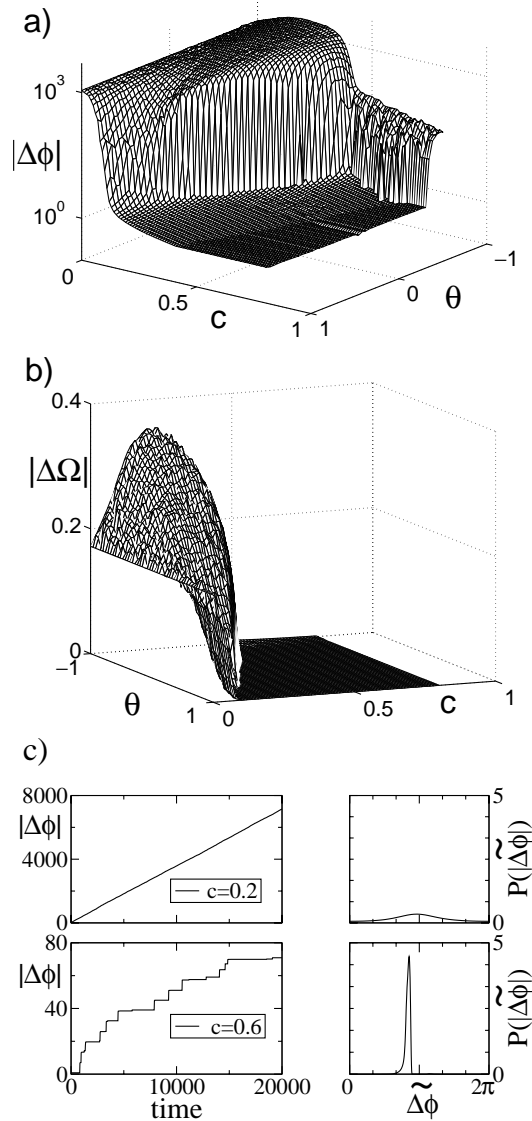
a)

b)

c)

FIG. 4.   (a) Maximum value of $|\Delta\phi(t)|$ (in logarithmic scale) over the finite time $t = T + 6000$ vs the parameter space (c, θ); (b) absolute value of $\Delta\Omega$ vs the parameter space (c, θ); (c) $|\Delta\phi|$ vs time for $c = 0.2$ (upper left) and $c = 0.6$ (lower left) with $\theta = -0.9$. Note that the function in the lower plot is increasing by finite jumps (2π phase slips), while in the upper plot the phase difference increases linearly with time reflecting a non-vanishing mean frequency mismatch. Upper (lower) right plots report $P(\widetilde{\Delta\phi})$ vs $\widetilde{\Delta\phi}$ (see text for definitions).

chaotic fields influenced by an asymmetry in the coupling. In particular, we have given evidence of novel features induced by asymmetry, such as the setting of the thresholds for the appearance of FS, PS, and CS, as well as the selection of the final synchronized state and of the transition route to it.

[1] A. Pikovsky, M. Rosenblum, and J. Kurths, *Synchronization: A Universal Concept in Nonlinear Sciences* (Cambridge University Press, Cambridge, 2001); S. Boccaletti, J. Kurths, G. Osipov, D. Valladares, and C. Zhou, Phys. Rep. **366**, 1 (2002).

[2] C. Schafer *et al.*, Nature (London) **392**, 239 (1998); P. Tass *et al.*, Phys. Rev. Lett. **81**, 3291 (1998); G. D. Van Wiggeren and R. Roy, Science **279**, 1198 (1998); A. Neiman *et al.*, Phys. Rev. Lett. **82**, 660 (1999); D. J. DeShazer *et al.*, Phys. Rev. Lett. **87**, 044101 (2001).

[3] C. M. Ticos *et al.*, Phys. Rev. Lett. **85**, 2929 (2000); D. Maza *et al.*, Phys. Rev. Lett. **85**, 5567 (2000); E. Allaria *et al.*, Phys. Rev. Lett. **86**, 791 (2001).

[4] S. H. Strogatz, S. E. Mirollo, and P. C. Matthews, Phys. Rev. Lett. **68**, 2730 (1992); A. Pikovsky, M. Rosenblum, and J. Kurths, Europhys. Lett. **34**, 165 (1996); G. Osipov *et al.*, Phys. Rev. E **55**, 2353 (1997); V. N. Belykh, I. Belykh, and E. Mosekilde, Phys. Rev. E **63**, 036216 (2001).

[5] V. N. Belykh and E. Mosekilde, Phys. Rev. E **54**, 3196 (1996); M. Hasler, Yu. Maistrenko, and E. Mosekilde, Phys. Rev. E **58**, 6843 (1998); A. Pikovsky, O. Popovich, and Yu. Maistrenko, Phys. Rev. Lett. **87**, 044102 (2001).

[6] G. Hu and Z. Qu, Phys. Rev. Lett. **72**, 68 (1994); L. Kocarev, Z. Tasev, and U. Parlitz, Phys. Rev. Lett. **79**, 51 (1997); R. O. Grigoriev, M. C. Cross, and H. G. Schuster, Phys. Rev. Lett. **79**, 2795 (1997); H. Chaté, A. Pikovsky, and O. Rudzick, Physica (Amsterdam) **131D**, 17 (1999).

[7] S. Boccaletti *et al.*, Phys. Rev. Lett. **83**, 536 (1999); J. Bragard, S. Boccaletti, and F. T. Arecchi, Int. J. Bifurcation Chaos Appl. Sci. Eng. **11**, 2715 (2001).

[8] L. Junge and U. Parlitz, Phys. Rev. E **62**, 438 (2000).

[9] See M. Cross and P. Hohenberg, Rev. Mod. Phys. **65**, 851 (1993), and references therein.

[10] P. Coullet, L. Gil, and F. Roca, Opt. Commun. **73**, 403 (1989).

[11] P. Kolodner, S. Slimani, N. Aubry, and R. Lima, Physica (Amsterdam) **85D**, 165 (1995).

[12] Y. Kuramoto and S. Koga, Prog. Theor. Phys. Suppl. **66**, 1081 (1981).

[13] T. Leweke and M. Provansal, Phys. Rev. Lett. **72**, 3174 (1994).

[14] B. Shraiman *et al.*, Physica (Amsterdam) **57D**, 241 (1992); H. Chaté, Nonlinearity **7**, 185 (1994); in *Spatiotemporal Patterns in Nonequilibrium Complex Systems*, edited by P. E. Cladis and P. Palffy-Muhoray (Addison-Wesley, New York, 1995).

[15] B. Janiaud *et al.*, Physica (Amsterdam) **55D**, 269 (1992).

[16] W. H. Press *et al.*, *Numerical Recipes in Fortran 90* (Cambridge University Press, Cambridge, 1992).

[17] B. Blasius, E. Montbrió, and J. Kurths, Phys. Rev. E **67**, 035204(R) (2003).